Deep Learning Based Module Defect Analysis for Large-Scale Photovoltaic Farms

Xiaoxia Li, Qiang Yang, *Senior Member, IEEE*, Zhuo Lou, and Wenjun Yan, *Member, IEEE*

***Abstract*—The efficient condition monitoring and accurate module defect detection in large-scale photovoltaic (PV) farms demand for novel inspection method and analysis tools. This paper presents a deep learning based solution for defect pattern recognition by the use of aerial images obtained from unmanned aerial vehicles. The convolutional neural network is used in the machine learning process to classify various forms of module defects. Such a supervised learning process can extract a range of deep features of operating PV modules. It significantly improves the efficiency and accuracy of asset inspection and health assessment for large-scale PV farms in comparison with the conventional solutions. The proposed algorithmic solution is extensively evaluated from different aspects, and the numerical result clearly demonstrates its effectiveness for efficient defect detection of PV modules.**

***Index Terms*—Unmanned aerial vehicles, photovoltaic farm inspection, convolutional neural network, pattern recognition.**

I. Introduction

With the increasing demand of low-carbon economy and technological advances, the photovoltaic (PV) energy generation has become one of the most important components of clean and renewable energy provision in the past decades. The statistics from the International Energy Agency (IEA) [1] indicated that the installed PV capacity in 2016 grew by 50% (over 74 GW) worldwide and China accounts for almost half of this expansion. The total global PV capacity is expected to reach 740 GW by 2022. However, such quick capacity expansion and reliability requirement of large-scale PV infrastructures impose an urgent demand for efficient asset assessment and early fault detection. In reality, such PV farms are often with large capacities (e.g., hundreds of MW, or even larger) and located in the remote sites without obvious sun shading, e.g., plains and hills, and spans over a large geographical area, as shown in Fig. 1. This brings direct challenges of efficient condition monitoring and fault diagnosis [2].

International Electrotechnical Commission (IEC) has investigated the reliability issue of photovoltaic (PV) technologies from different aspects and the importance of potential induced degradation (PID) detection has been highlighted. The timely and accurate identification of PV module defects can ensure adequate lifetime and efficient power generation of PV modules, and hence the reliable operation of overall large-scale PV farms [3], [4]. The conventional asset assessment tasks for PV farms are generally carried out by humans for individual PV modules. The module defects and failures are identified using electrical measurements (e.g., voltage, current and power), visual inspection, or thermographic analysis during system operation [5]. Obviously, such existing asset assessment and fault diagnosis methods are inefficient, even not feasible, to be adopted in large-scale PV systems in practice due to high error rate and long assessment time.

Fig. 1. An example of large-scale PV farms.

In literature, the automated remotely controlled systems have been adopted to achieve efficient condition monitoring and system maintenance for large-scale PV farms (e.g., [6], [7]). Through the adoption of unmanned aerial vehicles (UAVs), the inspection system can provide a non-destructive and reliable asset inspection and assessment (prognostic analysis and fault diagnosis) of large-scale PV farms with minimized human interventions [8]. The solution proposed in [8] aimed to automate the system inspection and prognostic functionalities based on the operational states of PV plant provided by a control system. The study in [9] implemented an infrared-thermography based solution using an unmanned aerial vehicle (UAV) platform and confirmed the effectiveness of PV plant inspection based on temperature profiles. In [10], an automatic defect detection method based on infrared thermography was implemented and evaluated. An UAV-mounted infrared thermography system was developed for efficient defect detection and location of PV panels

Manuscript received March 25, 2018; revised July 30, 2018; accepted September 24, 2018. Date of publication September 30, 2018; date of current version February 26, 2019. This work is supported in part by the Natural Science Foundation of China under Grant 51777183 and in part by the Natural Science Foundation of Zhejiang Province (LZ15E070001). Paper no. TEC-00301-2018. (*Corresponding author: Qiang Yang*.)

The authors are with the College of Electrical Engineering, Zhejiang University, Hangzhou 310027, China (e-mail: lixiaoxia@zju.edu.cn; qyang@zju.edu.cn; louzhuo@zju.edu.cn; yanwenjun@zju.edu.cn).

Color versions of one or more of the figures in this paper are available online at http://ieeexplore.ieee.org.

Digital Object Identifier 10.1109/TEC.2018.2873358

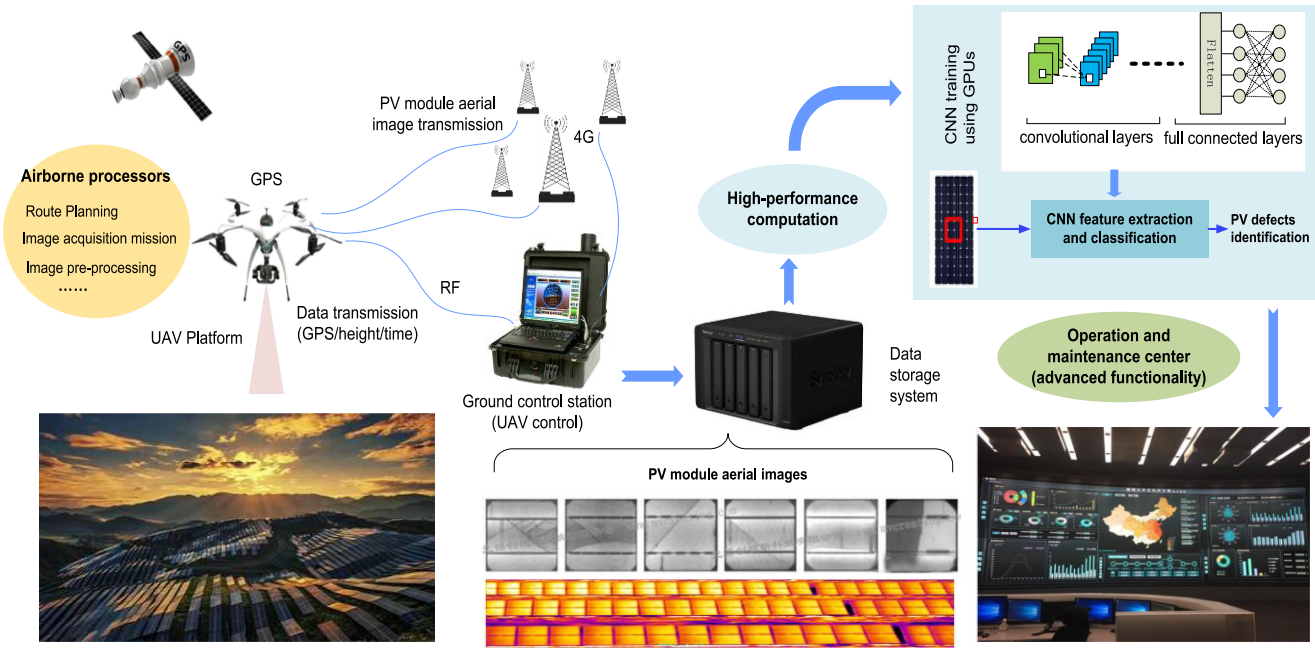

Fig. 2. UAV based intelligent inspection system for monitoring and fault detection of large-scale PV farms.

in [11]. The IR thermography based real-time analysis was presented for identification of potential defects of PV systems in [12]. Although such approach was confirmed to be efficient to hot-spot fault detection, it cannot perform analysis for other forms of faults. On the other hand, some research effort has exploited the UAV-based inspection platform with light cameras to obtain aerial images of PV modules to diagnose a variety of visible defects. The work in [13] studied the infrared scanning of PV solar plants and highlighted the benefit of using UAV based solution in comparison with the conventional ground assessment. The aerial thermo-visual photography based on the UAV platform was adopted in [14] to carry out the system inspection and fault detection tasks using image mosaicing techniques. In [15], an automatic solution based on aerial infrared imagery was developed for detection and analysis of temperature anomalies in photovoltaic modules, e.g., overheated modules, hot spots and overheated substrings. Our previous work [16] have exploited the diagnosis solution for two typical visible defects of PV modules, e.g., snail trails, dust-shading, through exacting the fault features from the obtained aerial images using the pattern recognition algorithms. However, it should be highlighted that the detection performance of such approach can significantly degrade if the obtained aerial images are with low resolution due to many reasons, e.g., wind effect and vehicle vibration. In summary, the accurate detection and analysis of various forms of PV module defects in large-scale PV farms demand a more efficient and robust pattern recognition solution for aerial images obtained during UAV inspection.

The deep convolutional neural network (CNN) has demonstrated strong capability of self-learning, fault tolerance and adaptability [20] and adopted in many fields, e.g., image classification and speech recognition [17]–[19]. With such recognition, the CNN based supervised learning solution can be adopted to analyze the aerial images of PV modules for defect detection and classification. In addition, the performance of CNN based pattern recognition can be significantly improved along with the increased data availability.

To this end, this paper exploits a novel approach for defect detection and analysis using CNN-based deep learning technique for aerial PV module images in the context of UAV based inspection of large-scale PV farms. The main technical contributions made in this work are summarized as follows: (1) an automatic UAV-based inspection system along with the CNN-based learning technique is developed for detection and analysis of various forms of visible module defects; and (2) the performance of the proposed solution is extensively evaluated from different aspects and compared with existing solutions through numerical experiments based on the aerial images collected from real PV farms. The numerical result clearly confirms the benefit of the proposed solution in efficient and accurate identification of different PV module defects.

The rest of the paper is organized as follows: Section II overviews the developed UAV-based inspection system for large-scale PV farms; the CNN based deep learning structure is presented in Section III; Section IV provides the implementation of the proposed solution in details and presents a set of key numerical results with discussions; and finally the conclusive remarks are given in Section V.

II. UAV-Based Inspection System

Fig. 2 illustrates the process of the proposed UAV-based inspection system and PV module defect diagnosis solution. Given the geographical information of the PV farms and the cruising scope, the airborne processor can plan an appropriate flight path and collect the aerial images of PV modules during the inspection process. The flight control of UAV is implemented at the Ground Control Station (GCS). The captured PV module

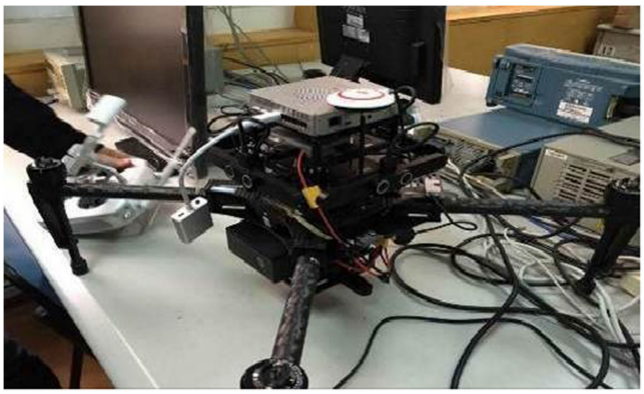

Fig. 3. UAV hardware platform and components.

TABLE I
UAV PLATFORM SPECIFICATION AND PARAMETERS

Parameter	Value
Cruise Speed	5–10 m/s
Operational range	1 Km
Mission Altitude	5~10m
Flight Endurance	0.25–0.67 h
Weight	3.6 Kg
Length(symmetric motor)	650mm
Wing span	0.3 m
Propulsion	Electric Power
Image sensor size	6.17 mm× 4.55 mm
Maximum resolution	4000×2250

images can be timely transmitted to GCS via 4G based wireless communication network for condition monitoring, and then made available to the data storage system that maintains the up-to-date image database. The available PV module images are used to characterize the features of module defects and failures through the machine-learning based algorithm in an offline fashion.

The performance of the adopted supervised learning based pattern recognition algorithm can be incrementally improved along with the increased availability of aerial images. It should be highlighted that, although the offline training process can take certain amount of time (e.g., a few hours) according to the adopted computation platform, the module defects can be identified by the well-trained model in a nearly real-time manor. This implies that such trained model can be programmed and integrated into the on-board processor of UAV platform for defect identification during PV farm inspection. The detection results can be made available to the operation and maintenance center (OMC) of PV farms.

In this work, the UAV-based inspection system is developed to carry out the tasks of aerial image acquisition and defect detection. The aerial PV module images are collected using a digital single-lens reflex (SLR) camera (Zenmuse X3) mounted on a light UAV (DJI Matrix100), as illustrated in Fig. 3. The detailed UAV specifications and parameters adopted in this work are presented in Table I. The airborne processor (Manifold) and wireless data transmission (LightBridge2) can implement

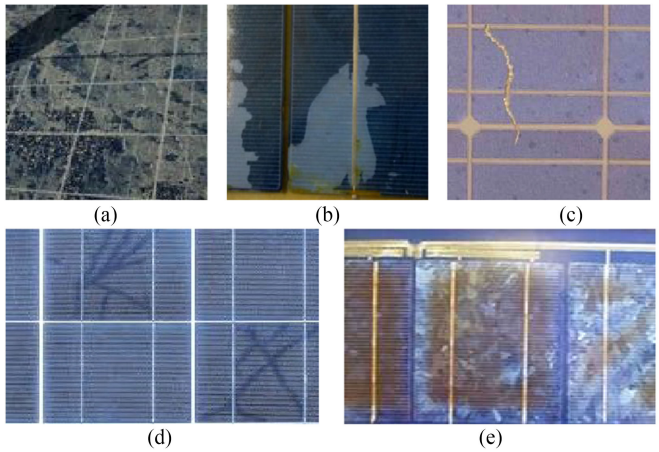

Fig. 4. Different forms of typical visible defects in PV modules: (a) Dust-shading; (b) Encapsulant delamination; (c) Gridline corrosion; (d) Snail trails; and (e) Yellowing.

efficient aerial image on-board processing and real-time image transmission.

Due to the long exposure outdoors, the PV modules are directly affected by various environmental factors, e.g., wind, salt, snow and dust, and different aging mechanisms can affect PV modules with correlated mismatching phenomena [21].

Fig. 4 illustrates the most common visible defects of PV modules, including the encapsulant delamination, dust shading, gridline corrosion, yellowing, and snail trails. The adherence loss among PV modules' layers can cause delamination. The severe encapsulant delamination can increase reflection and water penetration into the modules, resulting in the acceleration of cell oxidation and operational risks [22]–[24]. The accumulation of dust can directly reduce the light transmittance, and hence significantly undermine the photovoltaic power generation efficiency, sometimes can reduce by 50%, and even worse 80% [25]. The shading PV cells will lead to overheating to damage the modules [26], [27]. The snail trails might not directly deteriorate the power generation efficiency, but they are often associated with invisible cell cracks that lead to significant generation degradation [28]. The timely and accurate detection of module defects is considered of paramount importance to prevent PV farms from severe performance deterioration and operational failures.

III. PROPOSED CNN-BASED SOLUTION FOR DEFECT DIAGNOSIS

This section presents the proposed deep-learning based solution for PV module defect diagnosis in details. The idea behind the approach is to exact the deep features from the module images and carry out the pattern recognition of defects through the deep-learning neural network. It is known that the CNN is a feedforward neural network where each neuron merely affects the neurons in the adjacent layer and retains the spatial correlation of the images, and hence can capture local image characteristics. In CNN [29], [30], the alternating convolution and sub-sampling operations are firstly carried out, and the finally a generic multi-layer network is adopted. The output is

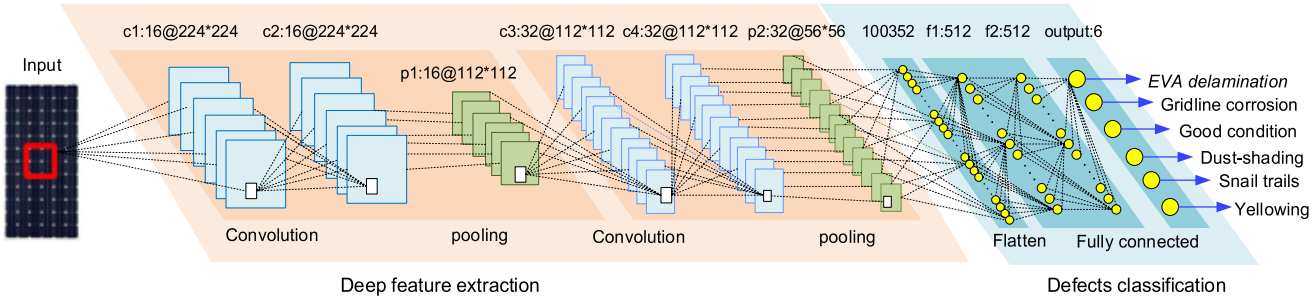

Fig. 5. The architecture of CNN feature extraction of PV module defects.

TABLE II
CNN STRUCTURE AND FEATURE EXTRACTION

Layer	Output shape	Parameters
Convolution (c1)	224, 224, 16	448
Convolution (c2)	224, 224, 16	2320
Max pooling (p1)	112, 112, 16	0
Convolution (c3)	112, 112, 32	4640
Convolution (c4)	112, 112, 32	9248
Max pooling (p2)	56, 56, 32	0
Flatten	100352	0
Fully connected (f1)	512	51380736
Fully connected (f2)	512	262656
Fully connected (output)	6	3078

flattened as a vector for the fully connected layer and softmax [31] is used to classify the obtained features into a number of corresponding classes.

A. Defect Classification Model

Fig. 5 illustrates the CNN structure adopted in this work that consists of 7 learned layers: four convolutional (c1∼c4) and three full connected layers (f1, f2 and output). The first 4 convolutional layers are used to extract CNN features by using 16, 16, 32 and 32 kernels (7*7*3), respectively. The training and testing features are extracted by the followed two fully connected layers (f1 and f2) that are both with 512 dimensions. The output of the last fully connected layer (i.e., f2) is fed to a 6-way classifier with the non-linear Rectified Linear Units (ReLU) [32] and can be further classified into 6 different class labels. In order to reduce the network computational complexity, the kernels of the second and fourth convolutional layers, i.e., c2 and c4, are followed by a max-pooling layer, respectively. The parameters of the adopted CNN structure are given in Table II.

B. Model Parameter Update

Here, the dataset of the collected PV module aerial images is denoted as $\{(x_1,\ y_1),\ (x_2,\ y_2),\ \ldots,\ (x_n,\ y_n)\}$, where n is the index of the module in the PV array, x represents the module image, and y denotes the corresponding class label. For the destination function, a squared-error loss function is adopted. It is a multiclass problem with m classes and q training examples. For a given sample, the cost function is expressed as (1).

$$E^n = \frac{1}{2}\sum_{k=1}^{m}(t_k^n - \mathrm{y}_k^n)^2 \tag{1}$$

For a training set with q samples, the cost function can be expressed as:

$$E^q = \frac{1}{2}\sum_{n=1}^{q}\sum_{k=1}^{m}(t_k^n - \mathrm{y}_k^n)^2 \tag{2}$$

where t_k^n is the k^{th} corresponding target (label) in sample n, and y_k^n is the value of output layer unit.

The network can be trained with the available dataset by stochastic gradient descent. In the training process, a momentum γ is introduced to accelerate the convergence or offset the gradient to prevent divergence [33]. A small amount of weight decay λ can reduce the model training errors. Through the gradient descent of error cost function parameters, the weight W updates with gradient descent based on (3) and (4).

$$W_{ij}^{l+1} = W_{ij}^{l} - \eta\frac{\partial E}{\partial W_{ij}^{l}} + v_{ij}^{l} \tag{3}$$

$$v_{ij}^{l+1} = \gamma v_{ij}^{l} - \lambda\eta w_{ij}^{l} \tag{4}$$

where η represents the learning rate, v is the momentum variable, W_{ij}^l and v_{ij}^l represent the weight and momentum between the unit i of layer l and the unit j of layer $l+1$, respectively. $\frac{\partial E}{\partial W_{ij}^l}$ is the gradient of the kernel weights.

The overall cost function is decreased constantly to update the parameters and build the ideal network according eq. (1)–(4).

Through the sharing weights and pooling, it could significantly reduce the computational complexity of the network and gradually build up further spatial and configurable invariance. The CNN parameters are updated aiming to produce more accurate defect predictions during the training process. The initialized hyperparameters of the CNN structure is given in Table III.

IV. EXPERIMENTAL ANALYSIS AND RESULTS

This section evaluates the proposed CNN-based approach for PV module defect analysis through extensive experiments from different aspects and compares its performance with existing solutions.

TABLE III
INITIALIZED HYPERPARAMETERS OF CNN ARCHITECTURE

Description	Symbol	Value
Patch size	p_s	16
Batch size	b_s	16
Gaussian kernel size	k	0.01
Learning rate	η	0.01
momentum	γ	0.9
weight decay	λ	0.01
Iteration times	T	400

TABLE IV
DIFFERENT CONDITIONS OF PV MODULES

Defect ID	PV module condition	Size of training samples	Size of validation samples	Size of test samples
#0	Dust shading	980	280	140
#1	Encapsulant delamination	980	280	140
#2	No defects	980	280	140
#3	Gridline corrosion	980	280	140
#4	Snail trails	980	280	140
#5	yellowing	980	280	140

A. Experimental Setup

Currently the dataset consisting of sufficient number of PV module images with different forms of defects can be barely obtained from the public domain. In this study, the collection of aerial PV module images are mainly obtained from three sources: PV module images collected during manual field inspection, generated synthesis module images with typical defects, and aerial module images obtained during UAV-based field inspection in three real PV farms: a PV farm (100 MW) in Datong, Shanxi Prov., a PV farm (100 MW) in Wuxi, Jiangxi Prov. and a PV farm (80 MW) in Taizhou, Zhejiang Prov., China.[1] The obtained aerial images are preprocessed before further analysis as they are inevitably with different degrees of noise and distortion, and captured with tilted angles. In this work, the image dataset consists of in total 8400 aerial image samples of PV modules under 6 different conditions (1400 samples for each condition), covering 5 different defect types (dust shading, encapsulant delamination, gridline corrosion, snail trails and yellowing, as mentioned in Fig. 4), as shown in Table IV.

The image samples are further divided into three subsets: training set (70%, i.e., 5880 samples), validation set (20%, i.e., 1680 samples) and test set (10%, i.e., 840 samples). The training set and validation set are used for parameter fitting through learning and tuning the parameters, respectively. Finally, the test set is used to assess the performance of the trained model for identification of different types of PV module defects.

[1]The PV module image dataset used in this work is available upon request.

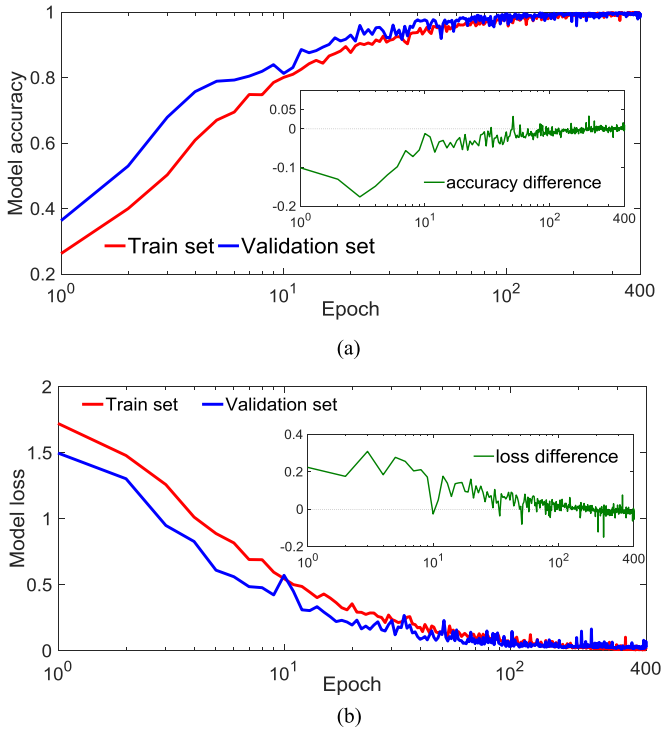

Fig. 6. Model performance assessment (a) model accuracy and (b) model loss function against the number of iterations.

In the experiments, the deep features are extracted from the 512-dimension fully connected layers, i.e., f1 and f2 (Table II), and the same learning rate is adopted for all convolution layers. Such CNN based feature extraction is implemented in python based on *tensorflow*. In addition, to accelerate the training, the non-saturating neurons and high-performance computation platform (with 4 NVIDIA TITAN GPUs) are used to carry out the convolution operation. The proposed CNN-based network is trained for about 400 cycles which take about 8 hours using the computation platform.

B. Training Process and Model Performance

The proposed CNN-based model is firstly assessed using the validation dataset before being adopted for defect identification and analysis of PV modules. Fig. 6 shows the model performance in terms of accuracy and loss function against the number of iterations during the training process. It shows that the training of the proposed CNN classifier can quickly converge for the validation image examples with the minimal error, which confirms the excellent generalization capability of the adopted network structure. The detection accuracy of the proposed model improves along with the increase of number of epochs, as shown in Fig. 6(a). It is also shown that the model loss decreases significantly along with the increase of number of iterations, and the loss reaches about 0.03 at the 100th iteration, as shown in Fig. 6(b). The obtained model after the training process can reach 98.5% identification accuracy for module defects. This indicates that a well-trained model can be obtained after a limited number of iterations with acceptable computational complexity.

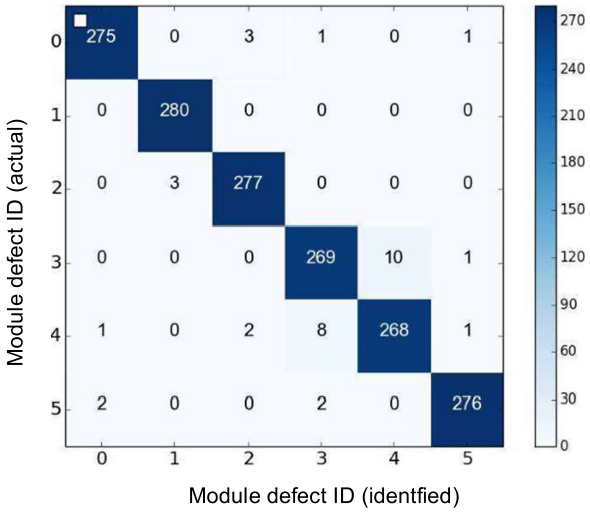

Fig. 7. Confusion matrix of defect classification using the trained model.

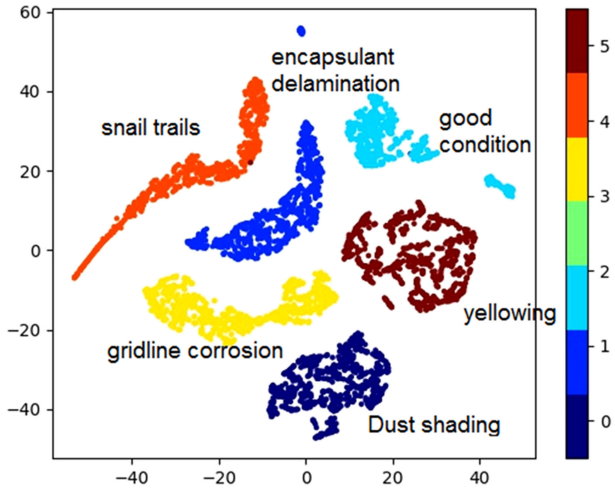

Fig. 8. *t*-SNE of learned features using the proposed training model for the validation set.

TABLE V
PERFORMANCE COMPARISON RESULT ON DIFFERENT PV DEFECTS

ID #0	ID #1	ID #2	ID #3	ID #4	ID #5
Dust shading	Encapsulant delamination	No defects	Gridline corrosion	Snail trails	Yellowing
98.2%	100%	98.9%	96.1%	95.7%	98.5%

The proposed CNN structure is evaluated for different operational conditions of PV modules and the numerical result is presented using a confusion matrix, as illustrated in Fig. 7. The confusion matrix presents the classification of all PV module conditions, and indicates the classification accuracy and misclassification error. The ordinate axis and horizontal axis of the confusion matrix refer to the actual defect types (ID #0∼#5) and the identified defect types, respectively. It can be clearly observed that the proposed solution can correctly identify different forms of PV module defects with high accuracy. The confusion matrix also shows that the gridline corrosion (ID #3) and snail trails (ID #4) are with lower detection accuracy, and hence more features are required to efficiently distinct these two types of defects.

Based on the aforementioned training model, the performance for PV defect identification is further assessed using 840 samples (i.e., 140 samples for each PV module condition). The numerical result presented in Table V demonstrates that all types of module defects can be identified with high accuracy (above 95%) with the mean accuracy of 97.9% for all module conditions.

In order to evaluate the capability of the proposed deep learning model for automatic extraction of PV module defect features, it is worth examining the layer features during the learning process. Due to the fact that the data features (512 dimensions) exacted from fully connected layers (i.e., f1 and f2) are all high-dimensional, the nonlinear dimensionality reduction method, t-Distributed Stochastic Neighbor Embedding (t-SNE), is adopted to analyze and visualize the learned features and highlight the useful hidden information in the original module images. Fig. 8 illustrates the exacted 512-dimention data features for 6 different PV module conditions (covering the case of no defect and 5 defect types) using *t*-SNE that can be clearly distinguished.

C. PV Defect Identification Performance Analysis

Here, the performance of the proposed CNN-based defect detection and analysis solution is assessed from different aspects, e.g., the performance against different parameter selections and sizes of image dataset, and evaluated in comparison with the existing solutions through a range of experiments.

Case 1: Performance With Different Parameter Selection

Impact of the network depth: The network structure can greatly affect the performance of the proposed solution. Hence, the performance against different number of convolution layers (each layer contains 16 feature maps) are firstly assessed through experiments to quantify the impact of network depth. Fig. 9(a) presents the result of mean test error of 840 prediction trials (i.e., the validation samples) for a range of models with different number of convolution layers, i.e., c1, c1c2, c1c2c3, c1p1c2p2, c1c2p1, c1p1c2p2c3p3 and c1c2p1c3c4p2. Fig. 9(b) shows the t-SNE result of the learned features for different models, the extracted data features from 6 categories in c1 spread the space and most of them overlap each other, which can be hardly distinguished. Comparing with model c1, c1c2 and c1c2c3, more convolution layers have not led to significant improvement in terms of detection accuracy and two convolution layers are considered sufficient in the evaluated case, as indicated from Fig. 9(b). The result shown in Fig. 9(c) indicates that the increase of the number of layers can introduce additional computational complexity, but hardly improve the accuracy of defect identification.

Impact of stochastic pooling: Added a pooling layer to the convolutional layers, it could significantly reduce the computational complexity of the network. Fig. 9(a) and (c) show the mean accuracy of the test dataset and the time consumption for defect detection, respectively. The evaluation is carried out with different pooling structure $(c_n p)_m$, like one convolutional layer

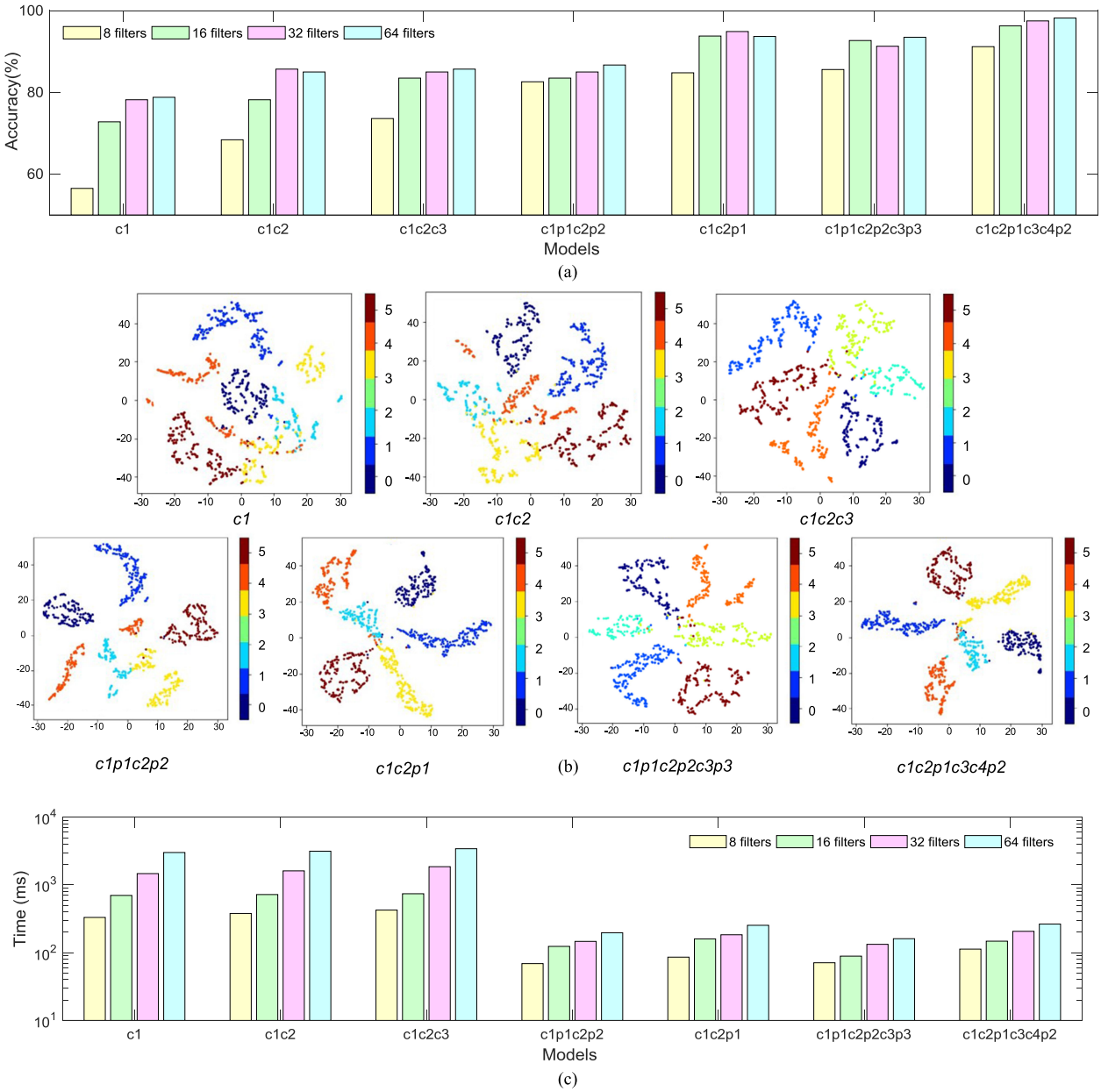

Fig. 9. The performance evaluation of identification trials using different models (a) the mean accuracy of defect detection; (b) t-SNE of learned features; and (c) the mean time consumption of defect detection.

with one pooling layer (c1p1), two convolutional layers with one pooling layer (c1c2p1). It can be seen that the mean test accuracy with pooling are higher than the convolutional layers only. Model c1p1c2p2 is more accurate than model c1c2, and the time consume has a significant reduction, shown as in Fig. 9(c). This is due to the fact that the pooling reduces the dimensionality, and hence stimulates the calculation of output weights.

In addition, the model c1c2p1 demonstrates better performance than model c1p1c2p2, the same as the model c1p1c2p2c3p3 and c1c2p1c3c4p2. This suggests that the $(c_2p)_m$ model structure is better than the $(cp)_m$ structure. In addition, the mean accuracy of model c1c2p1c3c4p2 is around 97%. Fig. 9(b) shows that the extracted features from aerial module images for different type of PV module conditions can be easily distinguished through the addition of pooling layers.

Fig. 9(c) clearly shows that the models with different number of filters can introduce different computational complexities with the computation time from hundreds of milliseconds to thousands of milliseconds, which are considered acceptable in practice.

Impact of number of filters: The result shown in Fig. 9(a) demonstrates that the detection accuracy of PV module defects can be significantly improved when the number of filters increased from 8 to 64, in particular for model c1 and c1c2. This indicates that a larger number of filters can enhance the capability of deep feature exaction of module defects. However, once the network depth is sufficient (more than two convolutional

TABLE VI
THE ACCURACY ALONG WITH THE DIFFERENT NUMBER SAMPLES

No. of samples	600	1200	1800	2400	3000	3600	4200
Accuracy (%)	15.33	16.25	15.84	18.1	21.17	17.8	19.4
No. of samples	4800	5400	6000	6600	7200	7800	8400
Accuracy (%)	26.5	91.2	**97.3**	**98.5**	**98.1**	**98.6**	**98.7**

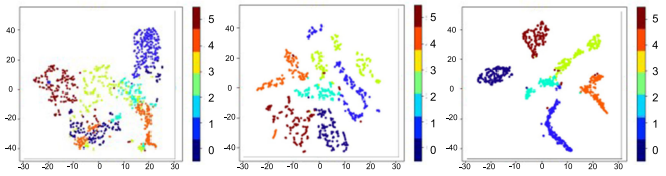

Fig. 10. t-SNE projection of the learned features using the proposed method. (a) raw data features (extracted by the first four convolutional layers); (b) features in the first fully connected layer; and (c) features in the second fully connected layer.

layers), e.g., model c1c2c3, c1c2p1, c1p1c2p2c3p3 and c1c2p1c3c4p2, no significant performance improvement can be obtained when the number of filter exceeds 16 filters, as shown in Fig. 9(a). Such observation implies that 16 filters are sufficient for the identification and analysis of module defects in this study work considering the introduced time complexity. Through the above analysis, it can be seen that the model c1c2p1c3c4p2 with 16 filters can meet the requirement of defect identification and make the best trade-off between the detection accuracy and the computational complexity.

Case 2: Performance With Different Dataset Sizes

This case evaluates the performance of the proposed solution for different dataset sizes, from 600 samples to 8400 samples. The result presented in Table VI shows the variation trends of the accuracy along with the different sizes of datasets. It shows that the performance of the network improves along with the increase of dataset size. In particular, once the dataset size reaches 6000 samples (i.e., 1000 samples per type of PV conditions), the significant performance improvement of the proposed solution is observed. In fact, the performance and adaptability of pattern recognition of PV module defects can be further improved once sufficient aerial image samples are available.

Case 3: Performance of the Learned Features in Different Layers

In order to illustrate the capability of the proposed deep learning based model in defect feature exaction from the aerial PV module images, the learning process is examined layer by layer in details. Fig. 10 presents the extracted deep features obtained by t-SNE, which can highlight the useful hidden information in the raw input data (original module aerial images).

Fig. 10(a) shows that the raw data features extracted after the first four convolutional layers are difficult to be distinguished among each other. Fig. 10(b) shows that the deep features obtained by t-SNE from the first fully connected level (i.e., f1) features can improve the identification performance in comparison with the raw data features. Further, the deep features from the second fully connected (i.e., f2) level features, as shown in Fig. 10(c), can clearly distinguish different defect features. It is shown that the higher level features can represent the measured signals more precisely than lower level features. Therefore, the evaluation clearly confirms the capability and adaptability of the proposed solution during the learning process.

TABLE VII
PERFORMANCE COMPARISON FOR DIFFERENT PV DEFECTS

Defect type	Conventional solution [16]	Pre-trained Vgg16 [17]	The proposed solution
Dust shading	89.7%	76.3%	97.8%
Encapsulant delamination	77.5%	68.6%	99.5%
No defects	86.8%	89.4%	98.5%
Gridline corrosion	47.9%	67.6%	98.0%
Snail trails	48.3%	67.9%	97.8%
yellowing	96.8%	73.5%	98.1%

Case 4: Performance Comparison With Conventional Solution

Finally, the performance of the proposed CNN based solution is further evaluated in comparison with the conventional pattern recognition algorithm [16] and the pre-trained Vgg16 in ImageNet [17].

Table VII presents the comparative result for identifying different types of PV module defects based on the adopted image dataset. It is shown that the conventional pattern recognition algorithm suggested in [16] can perform well for the defects of dust shading and yellowing with the accuracy of 89.7% and 96.8%, respectively, through extracting the defect features from the available image samples. However, the diagnosing performance of such approach can significantly degrade for certain PV module defects with similar characteristics, e.g., snail trails and gridline corrosion with detection accuracy of 48.3% and 47.9%, respectively, due to limited adaptability and robustness.

For the pre-trained Vgg16 [17], it is firstly used to extract the off-the-shelf features of the PV modules from the hidden fully-connected layers before carrying out the defect classification using the SVM classifier. It is shown that the pre-trained Vgg16 can provide improved performance in detection and analysis of snail trails and gridline corrosion than the conventional pattern recognition solution [16]. However, such performance is still considered not sufficiently reliable and accurate for all typical module defects to meet the inspection requirement. The numerical result shown in Table VII clearly confirms that the proposed solution outperforms in all evaluated cases for diagnosis of different module defect scenarios with high accuracy above 97%.

V. CONCLUSIONS AND DISCUSSIONS

This paper presented an automatic UAV-based inspection system with the CNN deep-learning based defect diagnosis

functionality to assess the operational condition of modules during the inspection of large-scale PV farms. The proposed defect detection and analysis solution is extensively evaluated against the existing solutions through a comparative study. The numerical result clearly confirms its effectiveness in diagnosing different forms of typical defects of PV modules, including dust shading, encapsulant delamination, gridline corrosion, snail trails and yellowing, with high accuracy. Such module assessment approach can be carried out in a real-time fashion with the well-trained model, and hence can be integrated on-board in the UAV platform for efficient inspection of large-scale PV farms with minimized implementation hurdles.

With the respect of future work, a number of research directions are considered worth further research and implementation effort. The offline trained defect detection model can be programmed into the airborne processor of UAV platform so as to carry out the real-time defect detection during inspection process. The reliability and robustness of the proposed UAV-based inspection system along with the deep-learning defect detection solution needs to be further validated and improved through extensive field assessments. In addition, the data analysis of the real-time electrical measurements of operating PV modules obtained from the underlying system monitoring infrastructure can be used in conjunction with the proposed solution to further improve the performance of asset inspection and assessment.

REFERENCES

[1] International Energy Agency, "Renewables 2017" 2017. [Online]. Available: http://www.iea.org/renewables/

[2] S. Tatapudi *et al.*, "Defect and safety inspection of 6 PV technologies from 56,000 modules representing 257,000 modules in 4 climatic regions of the United States," in *Proc. IEEE 43rd Photovolt. Spec. Conf.*, Washington, DC, USA, Jun. 2016, pp. 1747–1751.

[3] H. Denio, "Aerial solar thermography and condition monitoring of photovoltaic systems," in *Proc. IEEE 38th Photovolt. Spec. Conf.*, Austin, TX, USA, Jun. 2012, pp. 000613–000618.

[4] M. Köntges *et al.*, "Review of failures of photovoltaic modules," Int. Energy Agency, Paris, France, Rep. IEA-PVPS T13-01:2014, 2014.

[5] M. Munoz, M. Alonso-Garcia, N. Vela, and F. Chenlo, "Early degradation of silicon PV modules and guaranty conditions," *Sol. Energy*, vol. 85, no. 9, pp. 2264–2274, Sep. 2011.

[6] J. Tsanakas, L. Ha, and F. Al Shakarchi, "Advanced inspection of photovoltaic installations by aerial triangulation and terrestrial georeferencing of thermal/visual imagery," *Renewable Energy*, vol. 102, pp. 224–233, Mar. 2017.

[7] F. Grimaccia, S. Leva, and A. Niccolai, "PV plant digital mapping for modules defects detection by unmanned aerial vehicles," *IET Renewable Power Gener.*, vol. 11, no. 10, pp. 1221–1228, Aug. 2017.

[8] M. Aghaei, F. Grimaccia, C. Gonano, S. Leva, "Innovative automated control system for PV fields inspection and remote control," *IEEE Trans. Ind. Electron.*, vol. 62, no. 11, pp. 7287–7296, Aug. 2015.

[9] C. Buerhop, T. Pickel, M. Dalsass, H. Scheuerpflug, C. Camus, and C. J. Brabec, "aIR-PV-check: A quality inspection PV-power plants without operation interruption," in *Proc. IEEE 43rd Photovolt. Spec. Conf.*, Portland, OR, USA, Jun. 2016, pp. 1677–1681.

[10] X. Gao *et al.*, "Automatic solar panel recognition and defect detection using infrared imaging," *Proc. SPIE*, vol. 9476, May 2015, Art. no. 947600.

[11] P. Zhang *et al.*, "Detection and location of fouling on photovoltaic panels using a drone-mounted infrared thermography system," *J. Appl. Remote Sens*, vol. 11, Feb. 2017, Art. no. 016026.

[12] M. Aghaei A. Gandelli, F. Grimaccia, S. Leva, and R. E. Zich, "IR real-time analyses for PV system monitoring by digital image processing techniques," in *Proc. Int. Conf. Event-Based Control, Commun., Signal Process*, Krakow, Poland, USA, Jun. 2015, pp. 1–6.

[13] T. Kauppinen *et al.*, "About infrared scanning of photovoltaic solar plant," *Proc. SPIE*, vol. 9485, May 2015, Art. no. 948517.

[14] M. Aghaei, S. Leva, and F. Grimaccia, "PV power plant inspection by image mosaicing techniques for IR real-time images," in *Proc. IEEE 43rd Photovolt. Spec. Conf.*, Portland, OR, USA, Jun. 2016, pp. 3100–3105.

[15] S. Dotenco *et al.*, "Automatic detection and analysis of photovoltaic modules in aerial infrared imagery," in *Proc. IEEE Winter Conf. Appl. Comput. Vis.*, Lake Placid, NY, USA, Mar. 2016, pp. 1–9.

[16] X. Li *et al.*, "Visible defects detection based on UAV-based inspection in large-scale photovoltaic systems," *IET Renewable Power Gener.*, vol. 11, pp. 1234–1244, Aug. 2017.

[17] K. W. Kim, H. G. Hong, G. P. Nam, K. R. Park., "A study of deep CNN-based classification of open and closed eyes using a visible light camera sensor," *Sensors*, vol. 17, Jun. 2017, Art. no. 21.

[18] W. Zhao *et al.*, "Superpixel-based multiple local CNN for panchromatic and multispectral image classification," *IEEE Trans. Geosci. Remote Sens.*, vol. 55, no. 7, pp. 4141–4156, Jul. 2017.

[19] J. Acquarelli, T. Laarhoven, and J. Gerretzen, "Convolutional neural networks for vibrational spectroscopic data analysis," *Anal. Chim. Acta*, vol. 954, pp. 1873–4324, Feb. 2017.

[20] S. Hoo-Chang *et al.*, "Deep convolutional neural networks for computer-aided detection: CNN architectures, dataset characteristics and transfer learning," *IEEE Trans. Med. Imag.*, vol. 35, no. 5, pp. 1285–1298, May 2016.

[21] S. Mohammed, B. Boumediene, and B. Miloud, "Assessment of PV modules degradation based on performances and visual inspection in Algerian Sahara," *Int. J. Renewable Energy Res.*, vol. 6, no. 1, pp. 106–116, Jan. 2016.

[22] A. Bouraiou *et al.*, "Analysis and evaluation of the impact of climatic conditions on the photovoltaic modules performance in the desert environment," *Energy Convers. Manage.*, vol. 106, pp. 1345–1355, Dec. 2015.

[23] A. Skoczek, T. Sample, E. Dunlop, and H. Ossenbrink, "Electrical performance results from physical stress testing of commercial PV modules to the IEC 61215 test sequence," *Sol. Energy Mater. Sol. Cells*, vol. 92, pp. 1593–1604, Dec. 2008.

[24] J. Tracy, N. Bosco, and R. Dauskardt, "Encapsulant adhesion to surface metallization on photovoltaic cells," *IEEE J. Photovolt.*, vol. 7, no. 6, pp. 1635–1639, Nov. 2017.

[25] A. Tabanjat, M. Becherif, and D. Hissel, "Reconfiguration solution for shaded PV panels using switching control," *Renewable Energy*, vol. 82, pp. 4–13, Oct. 2015.

[26] A. Dolara *et al.*, "Experimental investigation of partial shading scenarios on PV (photovoltaic) modules," *Energy*, vol. 55, pp. 466–475, Jun. 2015.

[27] M. Bressan *et al.*, "A shadow fault detection method based on the standard error analysis of I-V curves," *Renewable Energy*, vol. 99, pp. 1181–1190, Dec. 2016.

[28] A. Dolara, G. C. Lazaroiu, S. Leva, G. Manzolini, and L. Votta, "Snail trails and cell micro-cracks impact on pv module maximum power and energy production," *IEEE J. Photovolt.*, vol. 6, no. 5, pp. 1269–1277, Sep. 2016.

[29] A. Manoj, C. Han, F. Michael, and P. Milder, "Fused-layer CNN accelerators," in *Proc. 49th Annu. IEEE/ACM Int. Conf. Microarchit.*, Taipei, Taiwan, Oct. 2016, Art. no. 22.

[30] K. Simonyan and A. Zisserman, "Very deep convolutional networks for large-scale image recognition," in *Proc. Int. Conf. Comput. Vis. Pattern Recognit.*, Apr. 2015, pp. 730–734.

[31] W. Liu, Y. Wen, Z. Yu, and M. Yang, "Large-margin softmax loss for convolutional neural networks," in *Proc. Int. Conf. Mach. Learn.*, New York, NY, USA, Nov. 2017, pp. 507–516.

[32] X. Jiang *et al.*, "Deep neural networks with elastic rectified linear units for object recognition," *Neurocomputing*, vol. 275, pp. 1132–1139, Feb. 2018.

[33] A. Botev, G. Lever, and D. Barber, "Nesterov's accelerated gradient and momentum as approximations to regularized update descent," in *Proc. Int. Joint Conf. Neural Netw.*, Anchorage, AK, USA, May 2017, pp. 1899–1903.

Xiaoxia Li received the B.S. degree in automation in 2015 from Zhejiang University, Hangzhou, China, where she is currently working toward the Ph.D. degree in control theory and control engineering. Her research interests include image analysis, renewable energy analysis and modeling, fault detection, and unmanned aerial vehicles.

Qiang Yang (M'03–SM'18) received Ph.D. degree in electronic engineering and computer science from Queen Mary, University of London, London, U.K., in 2007. From 2007 to 2010, he was with the Department of Electrical and Electronic Engineering, Imperial College London, London, U.K. He visited University of British Columbia and University of Victoria Canada as a Visiting Scholar in 2015 and 2016. He is currently an Associate Professor with College of Electrical Engineering, Zhejiang University, Hangzhou, China, and has published more than 150 technical papers, applied 50 national patents, coauthored 3 books and several book chapters. His research interests over the years include communication networks, smart energy systems, and large-scale complex network modeling, control and optimization. He is the Senior Member of the IET and the Senior Member of the China Computer Federation.

Zhuo Lou received the B.S. degree in automation in 2016 from Zhejiang University, Hangzhou, China, where she is currently working toward the master's degree in control theory and control engineering. Her research interests include image analysis, computer vision and unmanned aerial vehicles.

Wenjun Yan received the M.Sc. and Ph.D. degrees from Zhejiang University, Hangzhou, China, in 1991 and 1994, respectively. He is currently a Full Professor with the College of Electrical Engineering, Zhejiang University. His research interests include robust control, fault diagnose for hybrid systems, home service robotics and coordinated dispatch for electricity and heat in microgrids.